RSC Advances



This is an *Accepted Manuscript*, which has been through the Royal Society of Chemistry peer review process and has been accepted for publication.

Accepted Manuscripts are published online shortly after acceptance, before technical editing, formatting and proof reading. Using this free service, authors can make their results available to the community, in citable form, before we publish the edited article. This Accepted Manuscript will be replaced by the edited, formatted and paginated article as soon as this is available.

You can find more information about *Accepted Manuscripts* in the **Information for Authors**.

Please note that technical editing may introduce minor changes to the text and/or graphics, which may alter content. The journal's standard <u>Terms & Conditions</u> and the <u>Ethical guidelines</u> still apply. In no event shall the Royal Society of Chemistry be held responsible for any errors or omissions in this *Accepted Manuscript* or any consequences arising from the use of any information it contains.



CdS nanorods - MFe₂O₄ (M = Zn, Co and Ni) nanocomposites: A heterojunction synthesis strategy to mitigate the environmental deterioration

Charanjit Singh^a, Devika^a, Rupal Malik^a, Vinod Kumar^b, and Sonal Singhal^a*

Abstract

A facile strategy to encrust MFe₂O₄ (M = Zn, Co and Ni) nanoparticles over CdS nanorods via two-step solvothermal method have been reported. The ferrite-CdS nanocomposites (NCs) were characterized using powder X-ray Diffraction (XRD) and Fourier Transform Infrared (FT-IR) spectroscopy. A shifting in the peak corresponding to (311) plane confirmed the presence of different metal ion in the spinel ferrite lattice. However, no variation in the peak of CdS was observed which stipulate that phase and morphology of CdS nanorods remain unaltered after hydrothermal treatment. High Resolution Transmission Electron Microscopy (HR-TEM) analysis revealed the efficacious attachment of the nanoferrite on the CdS nanorods. Optical studies of the NCs samples provided the information about the fabrication of visible light responsive photocatalyst and covered the solar spectrum from 525 nm to 737 nm. On the basis of magnetic studies, CdS-CoFe₂O₄ and CdS-NiFe₂O₄ were found to be ferromagnetic in nature with saturation magnetization of 26.4 and 15.5 emu/g respectively. Interestingly, a transition from ferromagnetic to super-paramagnetic was observed for ZnFe₂O₄ loaded CdS nanorods. The photo-catalytic activities of nanocomposites were studied by carrying out the photodegradation of rhodamine B and methylene blue dye under visible-light irradiation. Maximum activity was observed in case of CdS-ZnFe₂O₄ nanocomposites.

Keywords: Nanoferrite; Nanocomposites; Photoluminescence; Magnetism.

^a Department of Chemistry, Panjab University, Chandigarh-160014, India

^b Icon Analytical Equipment (P) Ltd., Mumbai, 400018, India

1. Introduction

In the last decade, multicomponent nanomaterials have gained considerable attention by the scientific community due to their unique electrical, optical and magnetic properties. 1-3 Consequently, such hybrid nanomaterials have shown caliber in diverse applications such as drug carriers, medical diagnosis, optoelectronic devices, lithium ion batteries and heterogeneous photocatalysis. 4-6

Various semiconductors nanomaterials such as TiO₂, SnO₂, BiVO₄, ZrO₂, ZnO, ZnS, CdS, WO₃, graphene and C₃N₄ has been coated with suitable metal nanoparticles (NPs) of Au, Ag, Ni, Pt, Rh and Cu which facilitates the interfacial charge transfer. These heterostructure nanomaterials accelerate the photo-degradation of noxious organic pollutants and photocatalytic splitting of water to produce hydrogen gas. Anyhow, these materials limit their application due to their non-magnetic nature and deprivation of visible light responsive behavior. Secondly, these noble metals are expensive and scarce. Therefore, it is of great interest to replace them with highly efficient and economic green magnetic materials. But, magnetic NPs have been found to be inactive in visible region until the generation of Fenton's reagent as previously reported. So, in order to play on these magnetic materials in visible light spectrum, such magnetite nanomaterials have been encrusted over the visible solar spectrum sensitive luminescent moieties.

CdS is most important II-VI semiconductor which has a band gap of 2.4 eV and absorbs the visible portion of the solar spectrum. However, the rapid recombination rate of the electron-hole pair retards their photocatalytic efficiency and enhances their photocorrosion.¹² In order to alleviate these limitations, visible light driven CdS/MFe₂O₄ (M = Fe, Zn, Co, Ni and Cu) luminescent magnetic materials have gained prominence as a frontline solution for the oxidation of toxic organic pollutant and dyes through photocatalysis.

Synthetic protocol of such heterostructure nanocomposites (NCs) deals with the consecutive growth of one component over the pre-synthesized domain or simultaneous growth of two different NPs domain in one pot reaction. Confined core-shell structure and layered distribution of one component over other distinctively shaped nanostructures (nanorod, nanosphere and nanocube) bestow them with extraordinary properties. Such multicomponent nanostructures behave as a single entity which retains the properties of all components. However, the nanorod (NR) core/shell heterostructure renders the incessant electron transport pathways due to high aspect ratio of NRs, minimal aggregation of NPs on NR surface and good surface contact. Hence, this phenomenon mitigates the recombination charges as compared to other core/shell structures leading to enhanced efficacy in the visible light irradiation.

However, tailoring of these different moieties is also a vanguard challenge so as to make effective contact between heterojunction materials. Roychowdhury et al. 16 synthesized fluorescent-magnetic CdS-Fe₃O₄ NCs with two step chemical route method. Magnetic measurements revealed the presence of super paramagnetic (SPM) behavior in the NCs at smaller particle size (5 to 7 nm) of Fe₃O₄ NPs whereas the NC with 12 nm Fe₃O₄ was essentially ferrimagnetic. Liu et al. 17 synthesized the CdS-Fe₃O₄ NCs with sonochemical method which exhibited good luminescent, magnetic and photocatalytic activity in visible light spectrum. Wang et al. 18 reported the epitaxial and non-epitaxial growth of α -Fe₂O₃ and Fe₃O₄ nanoparticles on the surface of CdS nanorods via polymer wrapping technique. Photocatalytic studies revealed that α -Fe₂O₃-CdS completely degrade the methylene blue dye in 7 h. However, only 62% of the dye was degraded using Fe₃O₄-CdS nanocomposite in same time interval; which could be due the blocking of the active sites of the catalyst by polyethylene glycol and polyvinylpyrrolidone binders.

In order to prevail above problems, this work reports a facile solvothermal method for the synthesis of MFe₂O₄ (M = Zn, Co and Ni) NPs-CdS NR heterostructure NCs. The synthesized samples were characterized via powder X-ray diffraction (XRD), Fourier transform infrared (FT-IR) spectroscopy. Transmission electron microscopy (TEM) was employed to analyze the shape and structure of the nanostructures whereas high resolution transmission electron microscope (HR-TEM) was used to scrutinize the heterojunction contact surface. Energy dispersive X-ray (EDX) revealed the information about elemental stoichiometry. Scanning tunneling electron microscope (STEM) with attached EDX elemental mapping was analyzed for the Zn, Fe, O, Cd and S elements proportionality in the sample. Further optical and magnetic properties were investigated at room temperature. A comparative photocatalytic behavior of all the samples was also studied in the presence of visible light.

2. Experiment

2.1. Materials

Cadmium nitrate tetrahydrate (Cd(NO₃)₂.4H₂O, 99%), thiourea (NH₂CSNH₂, 99.9%), ethylenediamine (C₂N₂H₈, 98%), ferric nitrate (Fe(NO₃)₃.9H₂O, 98%), cobalt nitrate hexahydrate (Co(NO₃)₂·6H₂O, 97%), nickel nitrate hexahydrate (Ni(NO₃)₂.6H₂O 98%), zinc nitrate hexahydrate (Zn(NO₃)₂·6H₂O, 99%) sodium hydroxide (NaOH, 98%), rhodamine B (99.7%) and methylene blue (99.2%) were purchased from Loba Chemicals and used without further purification. Absolute ethanol (C₂H₅OH, 99.9%), acetone (C₃H₆O, 98%) were purchased from Fisher Scientific. Deionized water was obtained using an ultrafiltration system (Milli-Q, Milipore) with the measured conductivity of 35 mho cm⁻¹ at 25 °C.

2.2. Physical measurements

The powder X-ray Diffractometer (XRD) X'Pert PRO, PANalytical, of scan type locked coupled, scan angle 20 - 80° range, scan step 0:02°, scan speed 3°/min, maximum power 40kV /40mA, Cu tube, T/T horizontal was used to analyze the phase purity of the synthesized samples. The scan time for each sample was about 20 minutes and the wavelength of Cu-Kα target was 1.5406 Å. The Fourier-Transform Infrared (FT-IR) spectra for all the samples were recorded by FTIR instrument (PERKIN ELMER) using KBr pellets in the range 4000-400 cm⁻¹. High Resolution Transmission Electron Microscope (HR-TEM) images, Energy Dispersive X-ray (EDX) and Scanning Tunneling Electron Microscope (STEM) were recorded using FEI Technai G2 F20 operated at 200 keV with magnification of 6 x 10⁶ times and resolution of 0.2 Å. The BET surface area analyzer ((11-2370) Gemini, Micromeritics, USA) was used to obtain the surface area of the samples which was operated in the temperature range of 10 °C – 350 °C. Prior to nitrogen adsorption measurements the samples were preheated at a temperature of 100 °C for 1 hr. Optical properties were analyzed using the UV-Vis spectrophotometer (Analytikjena SPECORD-205). Photo-irradiation was carried out using 160 W mercury lamp (96000 Lux) with a distance of 6 inches between the light source and the target surface.

2.3. Fabrication of CdS NRs

CdS NRs were fabricated via solvothermal process. In this typical synthesis, Cd(NO₃)₂.4H₂O (4.66 g) and thiourea (3.45 g) were added to 72 mL of ethylenediamine solvent. This reaction mixture was magnetically stirred for 30 min at room temperature followed by high temperature autoclaving for 24 h at 160 °C. Yellow colored precipitates so obtained were filtered and washed several times with acetone and distilled water. Further, this sample was dried overnight in vacuum oven at 60 °C. ¹⁹

2.4. Fabrication of $MFe_2O_4(M = Zn, Co \text{ and } Ni)\text{-}CdS NCs$

For the synthesis of CoFe₂O₄-CdS NCs, 400 mg of CdS NRs were dispersed in the 0.25M NaOH (50 mL) solution using ultrasonic bath sonicator for 30 minutes. Further, 20 mL of 0.05 M of Co(NO₃)₂·6H₂O and 0.1M Fe(NO₃)₃.9H₂O mixed solution was added drop wise to the above mixture. Brown colored precipitates appeared in the reaction mixture which was due to the formation of metal hydroxide. In order to obtain complete homogeneity, this mixture was magnetically stirred for 2 h. This mixture was further transferred into 100 ml capacity Teflon lined stainless steel autoclave and kept in the furnace at 180 °C for 12 h. Further, this mixture was allowed to cool down at room temperature followed by cleansing and purification of the sample with distilled water and acetone.²⁰ Due to the attachment of the magnetic moiety to the luminescent CdS NRs, an external magnet was used to clean and purify the sample without using the complex filtration process. Similar procedure was followed for the synthesis of ZnFe₂O₄-CdS NC's and NiFe₂O₄-CdS NC's.

2.5. Photocatalytic activity

Photocatalytic activities of pure CdS NRs and their corresponding CdS-MFe₂O₄ nanocomposites were scrutinized for the degradation of Rhodamine B (RhB) and methylene blue (MB) dye. For typical photo-catalysis reaction, 2.4 mg of RhB dye (100 mL) was degraded in the presence of visible light using 100 mg of the nanocatalyst. Before irradiation to the visible light, the sample was kept in dark for 30 minutes so as to achieve the adsorption/desorption equilibrium. Afterward, this dye solution was kept under the visible light lamp with continuous stirring. 2 mL aliquot was withdrawn after the regular intervals of time and catalyst was removed using external magnet. Subsequently, decolorization of dye was investigated with the help of UV-visible spectroscopy.

3. Results and discussion

3.1. Fourier transform infra-red (FT-IR) spectroscopy

The FT-IR spectra of pristine CdS NRs and their NCs with the ferrite NPs are depicted in Fig.1. All the peaks in the spectra match well with the values reported in the literature.²¹ It is evident from the figure, ferrite NPs garnered over the CdS NR surface displayed their fingerprint peaks at around 530-560cm⁻¹, which is ascribed to stretching vibration of tetrahedral M-O cluster. However, this peak was absent in pure CdS NRs sample. ZnFe₂O₄-CdS NCs offered Zn-O tetrahedral frequency at 536 cm⁻¹ whereas for CoFe₂O₄-CdS NCs, peak appeared at 560cm⁻¹ (see the inset of Fig.1.). NiFe₂O₄-CdS NCs also displayed peak at a vibrational frequency of 562cm⁻¹. This shifting in frequency can be rationalized in terms of reduced mass.²²

$$v^2 = k/_4 c^2 \pi^2 \mu \tag{1}$$

where v is frequency in cm⁻¹, k is the force constant, c is velocity of light and μ is the reduced mass. So, according to above equation, decrease in reduced mass results in an increase in vibrational frequency. Thus, shifting of peak towards higher vibrational frequency for cobalt and nickel ferrite NC are in good agreement with the above equation because of their lower molecular mass as compared to zinc ferrite NCs.

3.2. Powder X-ray diffraction (XRD) characterization

Fig. 2 shows the XRD pattern of CdS NRs and MFe₂O₄-CdS (M = Zn, Co and Ni) NCs. Peaks in the diffraction pattern of CdS NRs showing hexagonal phase (JCPDS-01-080-0006) of the nanostructure and planes of the CdS NRs match well with the previous literature.²³ Diffraction patterns of CdS-MFe₂O₄ (M = Zn, Co and Ni) NCs displayed the signature peaks for pristine CdS and corresponding spinel ferrite NPs, which were in good

agreement with JCPDS-01-089-1009, JCPDS-00-001-1121, JCPDS-01-074-208 for zinc, cobalt and nickel ferrite NCs respectively.²⁴ A shifting in the peak corresponding to lattice plane (311) was observed in NC samples. However, no variation in the lattice plane (102) of the CdS NRs was observed in all the samples as shown in the inset of the Fig 2. This implies that CdS NRs remain unaffected after the hydrothermal treatment. Shifting in the (311) plane of the nanocomposites samples was scrutinized using Le-bail refinement method. It was observed that lattice parameter of NCs sample decreased in order as follows:

$$CdS-ZnFe_2O_4(0.844 \text{ Å}) > CdS-CoFe_2O_4(0.838 \text{ Å}) > CdS-NiFe_2O_4(0.833 \text{ Å})$$

This change in lattice parameter was attributed to the presence of metal ions of different ionic radii in ferrite nanostructures

$$Zn^{2+}$$
 (88pm) > Co^{2+} (83.8 pm) > Ni^{2+} (73.1 pm)

Average crystallite size of the samples was calculated using Debye Scherrer equation²⁵:

$$d = \frac{K\lambda}{\beta\cos\theta} \tag{2}$$

where d is the average crystallite size, K is the shape factor approximated to 0.9, β is the line broadening at half the maximum intensity (at full width half of maximum intensity, FWHM), λ is the X-ray wave length. Broad and sharp peaks of the pristine CdS NRs and their corresponding NCs samples depict that sample are completely crystalline. Average crystallite size for the ferrite nanoparticles was calculated using the most intense (311) peak of the nanocomposite samples and are presented in table 1. As is clear from the table, the average crystallite size of the sample decreased as follows:

$$CdS$$
-NiFe₂O₄ > CdS -CoFe₂O₄ > CdS -ZnFe₂O₄

3.3. HR-TEM characterization

Size, shape and mode of attachment for CdS-ferrite heterojunction domains were scrutinized using HRTEM and STEM-point EDX characterization techniques. Scattered Area Electron Diffraction (SAED) pattern and lattice fringe width were also calculated to probe the crystallinity of the samples. Prior to analysis, annealed samples were dispersed in ethanol and sonicated for 10 minutes to obtain a clear dispersion. A drop of this suspension was put on the 400 mesh size carbon coated copper grid. As prepared specimen was thoroughly investigated under the electron beam to substantiate the formation of ZnFe₂O₄ NP encrusted CdS NRs heterostructure NCs. HR-TEM images shown in Fig 3 (a, b) manifested that CdS NRs have diameter around 50-70 nm and size of the zinc ferrite NPs were around 5-6 nm. As is clear from the images, a very fine layer of the zinc ferrite was coated on the CdS NRs and high resolution of around 2 nm revealed the information about the point of contact between the ferrite and CdS nano domains (See Fig 3(c)). Lattice fringes were calculated from the portrayed image and inter-planer distance between the two consecutive fringes was found to be around 0.25 nm for the (311) plane of the zinc ferrite NPs whereas CdS NRs exhibiting the distance of 0.33 nm for (102) plane. SAED pattern of the nanocomposite sample demonstrated the structural crystallinity and revealed the information about the (311) plane of zinc ferrite NPs along with the (102) plane of the CdS NRs (Fig 3(d)). Profile of frame portraying the inter-planer distance between consecutive fringes and fringe width obtained so far matches well with the XRD results (Fig 3(e, f)).

3.4. STEM point EDX analysis

For additional support STEM point EDX provided the information about the photoluminescence core with magnetite shell. Fig 4 (a) displays the 3-D vision of the CdS-ZnFe₂O₄ core-shell heterostructure in order to interpret the surface morphology and thickness

of shell. A point EDX spectroscopy acquired the signals of Cd, S, Zn, Fe and O from the selected frame of STEM image by positioning the electron beam on the center of the heterostructure. An additional signal for carbon and copper were also obtained due the TEM grid. No additional peak of any other impurity was observed which concluded that the samples so obtained were clean. Thus combinatorial effect of all the techniques make an unanimous conclusion that nanorod shaped luminescence CdS was ensheathed with zinc ferrite nanoparticles and a core-shell structure was achieved through this synthetic methodology with complete stoichiometric proportion of the nanocomposite sample.

3.5. BET Surface area analysis

The surface area of the nanocomposite samples were measured using the single point BET analyzer. All the samples were preheated at 100 °C for 1 hour before N_2 adsorption. Zinc ferrite - CdS nanocomposite sample was found to have maximum surface area value of 79.6 m²/gm. Surface area values measured for cobalt and nickel ferrite-CdS nanocomposite samples were found to be 54.5 and 24.4 m²/gm respectively.

3.6. Diffused UV-visible Reflectance Spectra and Band Gap of MFe₂O₄-CdS NC's

CdS NRs and ferrite NPs ensheathed CdS NRs were analyzed by diffused UV-visible reflectance spectroscopy to investigate their optical properties. Fig. 5 shows the band edge absorption spectra of pristine CdS NRs and their corresponding CdS-ferrite NCs. The absorbance results demonstrate that CdS NRs- MFe₂O₄ (M = Zn, Co and Ni) had significant absorbance in 525-725 nm wavelength range of the visible region which is important for photo catalytic reaction. Band edge absorption onset for CdS NRs was at 525 nm whereas for CdS NR-ZnFe₂O₄ NC the curve inclined towards the higher value of the onset absorbance around 600 nm. Further, encrustation of nickel and cobalt ferrite onto CdS NR increased the band edge absorbance.

In order to estimate the corresponding band gap energy, a plot of $(\alpha hv)^2$ vs photon energy (hv) was plotted (Fig. 6) The optical absorption coefficient near the band edge follows the equation²⁶:

$$\alpha h \nu = A \left(h \nu - E_g \right)^{1/2} \tag{3}$$

where α, h, ν, E_g, and A are the absorption coefficient, Plank constant, light frequency, band gap and proportionality constant, respectively. Band gap energy was deduced from this plot by drawing a normal to the linear part of the curve. A clear estimate about the onset absorbance and band gap value was driven from tauc's equation. Band gap value for the CdS NRs was found to be 2.35 eV. However, zinc, cobalt and nickel ferrite nanoparticles encrusted on CdS NRs displayed the band gap values around 2.22, 1.71 and 2.29 eV respectively. This indicated the significant change in the band energies due presence of different spinel structure of ferrite as well as the synergistic effect of attaching a small band gap material of ferrite NPs with large band gap CdS NRs. In comparison with the bulk band gap value for zinc, cobalt and nickel ferrite (1.92, 1.45 and 2.15 eV respectively), the red shift in the absorption edge was observed for all the ferrites which might be due to interface defects and the formation of sub-band-gap energy level in the nanocomposite material.²⁷

3.7. Magnetic properties of CdS-MFe₂O₄ NCs (M = Zn, Co and Ni)

Hysteresis loops for CdS-MFe₂O₄ NCs (M = Zn, Co and Ni) were investigated at 298 K using VSM by applying the external magnetic field between \pm 10 kOe and are shown in Fig. 7. From the plot between applied magnetic field and saturation magnetization it is clear that cobalt ferrite NPs wrapped on the CdS NRs shows maximum magnetization value (Table 2). This behavior of magnetization can be enlightened on the basis of Neel's two sub-lattice model. According to this model, the magnetic moment per formula unit in Bohr magneton $n_B^N(\chi)$ is expressed²⁸:

$$n_B^N(\chi) = M_B(\chi) - M_A(\chi) \tag{4}$$

where M_B and M_A are magnetization of B and A sub-lattices, respectively.

This behavior of saturation magnetization for CoFe₂O₄-CdS NCs is due to the strengthening of A-B interactions as the cobalt ion has a tendency to occupy octahedral B site. So, some of the Fe³⁺ ions get transferred to the tetrahedral site and the magnetic moment of M_B gets concerted. So, the saturation magnetization for the CoFe₂O₄-CdS NRs increased. However with the Zn²⁺ ions substituent, A-B exchange interactions weaken as Zn²⁺ ions have the tendency to occupy the tetrahedral A sites. So the magnetic moment of M_A gets diluted.²⁹ Therefore, for ZnFe₂O₄-CdS NCs, the curve didn't get saturated, indicating the fabrication of super-paramagnetic nanocomposites with negligible coercivity and remanance. However NiFe₂O₄-CdS NCs displayed ferromagnetic behavior. This superparamagnetic behavior of ZnFe₂O₄-CdS NCs can be attributed to lower particle size and the presence of non-magnetic ions in the spinel ferrite structure, which would have led to single domains.²⁹ These results are corroborated by the presence of single domain structure in HR-TEM images (Fig. 3)

A huge difference in magnetic parameters is also conspicuous from the hysteresis loops of the NCs. It is evident from the figure that the saturation magnetization value for the CdS-ZnFe₂O₄ NCs is 4.0 emu/g. However for CdS-CoFe₂O₄ NCs and CdS-NiFe₂O₄ NCs saturation magnetization is 26.4 and 15.5 emu/g respectively. Similarly, a vast variation in the values of remanance and coercivity was observed. The coercivity for CdS-ZnFe₂O₄ NCs was 8.5 Oe, which upsurged to 90 Oe and 377.2 Oe for CdS-NiFe₂O₄ NCs and CdS-CoFe₂O₄ NCs. On the similar line, remanance for ZnFe₂O₄-CdS NCs was found to be 0.005 emu/g and this value increased substantially for NiFe₂O₄-CdS NCs and CoFe₂O₄-CdS NCs respectively as shown in Table 2.

3.8. Photoluminescence (PL) properties

PL spectra of all the samples were recorded at an excitation wavelength of 260 nm, using 0.5 mg/mL of sample. Acetone was used for dispersing the samples, which due to its

protic nature manifested high intensity emission peaks.³⁰ As is evident from the Fig. 8., a strong PL peak at 535nm appeared for all the samples, along with weak intensity band at 595 nm and 652 nm. The appearance of intense peak can be ascribed to excitonic fluorescence caused by radiative electron-hole recombination of the detrapped electrons. The weak bands may be attributed to the trapped charge carrier at the defect site of the CdS NRs and CdS-MFe₂O₄NCs.³¹

It is also clear from the PL spectra that the band emission intensities decreased as CdS NRs were loaded with ferrite nanoparticles. Hence, ferrite nanoparticles serve as a p-type semiconductor whereas CdS nanorods work as n-type semiconductor. After the combination of these two distinctive moieties lead to the formation of p-n type heterojunction, which facilitate the migration of photo-induced electron and holes at the interface of MFe₂O₄-CdS NCs. ^{32,33} The variation band emission intensity followed the order as given:

$$CdS NRs > CdS-ZnFe_2O_4 > CdS-NiFe_2O_4 > CdS-CoFe_2O_4$$
.

The conduction band of MFe₂O₄ (M=Zn, Co, Ni) is more negative as compared to CdS. Also the valence band in case of CdS is more positive as compared to MFe₂O₄ (M=Zn, Co, Ni).³⁴ The light irradiation results into the creation of photo-induced electrons and holes. The photo-induced holes move towards MFe₂O₄ region and the photo-induced electrons drives in CdS region resulting into electron-hole separation. So, the CdS-Ferrite coupled system reduces the electron hole recombination resulting in quenching in emission intensity of the CdS-MFe₂O₄ as compared to pristine CdS NRs

3.9. Photocatalytic activity measurements

In photocatalytic degradation experiments, 100 mg of catalyst was added to 100 mL of RhB solution (24 mg/1000 mL) and MB solution (15 mg/1000 mL) which are considered as model pollutants. Before irradiation to the visible light lamp, the solutions were stirred for

half an hour in dark to achieve absorption/desorption equilibrium between the surface of the catalyst and dye molecules. Then, this solution was kept under the visible light illumination and 2.5 ml of aliquots were withdrawn after regular interval of time. Further, the catalyst was removed using external magnetic field and the dye sample was analyzed using UV-visible spectrophotometer. The control experiments, without any photo-catalyst, showed no noticeable decomposition of RhB indicating good photo stability of dye as shown in our previous reports. 35,36

Ferrite nanoparticles discretely are unable to oxidize the dye molecule in the visible region until the generation of the Fenton's reagent which is homogeneous in the dye solution. So, this system faces the difficulty in separation of homogeneous reagent and also has a drawback in quenching the effect of free radicals generated while analyzing the absorbance spectra of the dye solution. However, when these green magnetic nanoparticles were tailored with the visible light responsive moieties via creating a heterojunction, these magnetite materials became photoactive heterogeneously, easily separated by external magnet and the time consumption for the degradation of the dye molecules also reduces.

In presence of pure CdS NRs under visible light irradiation, the RhB dye was degraded in approximately 210 minutes. However, CdS NR-ZnFe₂O₄ NCs degraded the RhB dye molecule completely in 150 minutes. Also with CdS NRs, MB dye was degraded in 180 minutes. However, with the zinc ferrite-CdS NRs heterostructure, complete decolorization took place in 90 minutes. The percentage photocatalytic degradation was calculated by applying following equation³⁷:

%degradation =
$$\left(\frac{A_o - A_t}{A_o}\right) \times 100$$
 (5)

where A_0 is the initial concentration of dye and A_t is the concentration of dye at time t. The percentage degradation of MB and RhB in the presence of all the synthesized composites is shown in Fig 9 (a) and (b) respectively.

It is clear from the results that ZnFe₂O₄-CdS NCs show maximum efficiency in comparison to the pristine CdS NRs and their corresponding CoFe₂O₄ and NiFe₂O₄ NCs structures which can be attributed to the various factors.

Formation of smooth p-n heterojunction interface and the synergetic effect of the CdS and ferrite nanostructure are also responsible for the uniform transfer of the charges. In such heterojunction coupled system, photo-induced holes lean towards photo-chemically stable MFe₂O₄ region and the photo-induced electrons lean towards active CdS region resulting into electron-hole separation. Thus, photo-generated electrons and holes moves in reverse directions, reducing the recombination probability and enhancing the charge separation efficiency as can be seen from the decrease in the luminescent behavior with heterojunction as compared to the pristine CdS NRs.³⁸

So, following this mechanism, produced electrons react with the dissolved oxygen molecules to generate the superoxide anion radicals, whereas the holes are scavenged by the adsorbed water to form hydroxyl radicals. Superoxide anion and hydroxyl radical generated through this procedure decompose the chromophore of the dye molecules in to other molecules which diminishes the intensity of the absorbance spectra.³⁹

It is clear from the comparative Powder X-ray diffraction pattern of zinc ferrite loaded CdS NRs with cobalt and nickel ferrite NCs. Form the inset of fig. 2 it is found that (311) peak of the samples gets widened as we move from nickel to cobalt followed by zinc ferrite. This peak broadening indicates the reduction in the particle size of the zinc ferrite nanoparticle which ultimately reduces the surface area of the samples and hence leads to

activation of the catalyst at its maximum extent. Similar evidences are also observed form HRTEM and the superparamagnetic nature of the zinc ferrite loaded CdS NCs which could be due to single domain zinc ferrite NPs. BET surface area analysis also showed the maximum value of 79.6 m²/g for the zinc ferrite-CdS nanocomposite. So, increased surface area indicates the reduction in the particle size and enhanced photocatalytic activity of the zinc ferrite encrusted CdS nanorod samples.

Color of the samples shown in Fig. 2 changes form yellow to black with subsequent encrustation of the zinc, cobalt and nickel ferrite nanoparticles of the CdS NRs. Hence, as the color of the sample gets darker, the penetration of the visible light to the illuminated dye solution gets reduced due to the turbidity of the solution. Hence, photo activity of the samples decrease as the color of the samples darkened.³⁵

Zinc ferrite-CdS NCs has proved to be significant in photocatalysis, in comparison to the other NCs samples due to combining optical, magnetic and structural properties favoring the enhanced activity of the nanocomposite.

Future scope

In previous literature, hydrogen gas was generated through bio-waste materials by bacteria and enzymes which are temperature sensitive and very unstable. However, heterojunction NCs of magnetite and luminescent moieties can be advantageous in the field of water splitting using visible light responsive photoreactor with regeneration of the magnetically separable catalyst. These nanostructure moieties are proficient in magnetically guided drug loading and delivery due to their strong luminescent and magnetic behavior.

4. Conclusion

CdS nanorods-MFe₂O₄ (M = Co, Ni and Zn) nanocomposites (NCs) have been successfully synthesized using solvothermal route. The synthesized NCs have been characterized using powder XRD, FT-IR, HR-TEM, STEM-point EDX and optical spectroscopy. Surface area of CdS-ZnFe₂O₄, CdS-CoFe₂O₄ and CdS-NiFe₂O₄ NCs was found to be 79.6, 54.5 and 24.4 m²/g respectively. The potential of synthesized NCs as a photocatalyst have been explored by studying the degradation of Rhodamine B and Methylene Blue dyes. CdS nanorods-ZnFe₂O₄ NCs were found to be better photocatalyst than pristine ferrite and CdS nanorods and degraded the Rhodamine B and Methylene Blue dye in 120 and 90 min respectively.

Acknowledgements

The authors are grateful to Department of Science and Technology (DST) and Council of Scientific and Industrial Research (CSIR) for providing the necessary financial support. We are also highly thankful to Prof. K.B. Tikoo for the facilitating the HR-TEM Lab, National Institute of Pharmaceutical Education and Research (Mohali). The assistance of Kunash Instruments Pvt. Ltd., Thane (W), in performing surface area analysis of the samples is highly acknowledged. The authors are also grateful to SAIF, Panjab University, Chandigarh, in performing required sample analysis.

References

- P. Melinon, S. B. Colin, J. L. Duvail, F. Gauffre, N. H. Boime, G. Ledoux, J. Plain,
 P. Reiss, F. Silly and B. W. Fonrose, *Phys. Rep.*, 2014, 543 163-197.
- 2. L. Tong, X. Ding, X. Ren, X. Yang and H. Yang, *Dye Pigm.*, 2015, 113, 117-120.
- M. Cho, E. Q. Contreras, S. S. Lee, C. J. Jones, W. Jang and V. L. Colvin, *J. Phys. Chem. C.*, 2014, 118, 14606-14616.

- D. He, S. Wang, L. Lei, Z. Hou, P. Shang, X. He and H. Nie, *Chem. Eng. Sci.*, 2015, 125, 108-120.
- 5. J. Yu, J. Jin, B. Cheng and M. Jaronie, *J. Mater. Chem. A.*, 2014, 2, 3407-3416.
- K. Ramasamy, M. A. Malik, N. Revaprasadu and P. O'Brien, *Chem. Mater.*, 2013, 25, 3551-3569.
- 7. S. K. Das, T. Parandhaman, N. Pentela, A. K. M. Maidul Islam, A. B. Mandal and M. Mukherjee, *J. Phys. Chem. C.*, 2014, 118, 24623-24632.
- 8. J. Zhang, Y. Wang, J. Jin, J. Zhang, Z. Lin, F. Huang and J. Yu, *ACS Appl. Mater. Inter.*, 2013, 5, 10317-10324.
- R. Sahoo, A. Roy, C. Ray, C. Mondal, Y. Negishi, S. M. Yusuf, Anjali Pal and T.
 Pal, J. Phys. Chem. C., 2014, 118, 11485–11494.
- 10. C. Singh, A. Goyal and S. Singhal, *Nanoscale*, 2014, 6, 7959-7970.
- 11. C. Singh, S. Bansal, V. Kumar and S. Singhal, Ceram. Int., 2015, 41, 3595-3604.
- 12. X. Liu, Y. Yan, Z. Da, W. Shi, C. Ma, P. Lva, Y. Tang, G. Yao, Y. Wu, P. Huo and Y. Yan, *Chem. Eng. J.*, 2014, 241, 243-250.
- H. Qian, Y. Hu, Z. Li, X. Yang, L. Li, X. Zhang and R. Xu, J. Phys. Chem. C., 2010, 114, 17455–17459.
- 14. A. M. Balu, B. Baruwati, E. Serrano, J. Cot, J. Martinez, R. S. Varma and R. Luque, *Green Chem.*, 2011, 13, 2750-2758.
- 15. Y. Feng, I. Cho, P. M. Rao, L. Cai and X. Zheng, *Nano Lett.*, 2013, 13, 855-860.
- A. Roychowdhury, S. P. Patil, S. Kumar and D. Das, *Powder Technol.*, 2014, 254, 583-590.
- 17. X. Liu, Z. Fang, X. Zhang, W. Zhang, X Wei and B. Geng, *Cryst. Growth Des.*, 2009, 9, 197-202.

- L. Wang, H. Wei, Y. Fan, X. Gu and J. Zhan, J. Phys. Chem. C., 2009, 113, 14119-14125.
- 19. J. Ran, J. Yu and M. Jaronie, *Green Chem.*, 2011, 13, 2708-2713.
- L. Zhang, R. Zheng, Shuo. Li, B. K. Liu, D. J. Wang, L. L. Wang and T. F. Xie, ACS Appl. Mater. Interfaces, 2014, 6, 13406-13412.
- A. Goyal, S. Bansal, P. Samuel, V.Kumar and S. Singhal, *J. Mater. Chem. A.*, 2014,
 2, 18848-18860.
- 22. O. M. Hemeda, J. Magn. Magn. Mater., 2002, 251, 50-60.
- Z. Wu, H. Yu, L. Kuai, H. Wang, T. Pei and B. Geng, J. Colloid Interface Sci., 2014, 426, 83-89.
- A. Goyal, S. Bansal and S. Singhal, *Inter. J. Hydrogen. Energ.*, 2014, 39, 4895-4908.
- 25. R. P. Bagwe and K. C. Khilar, *Langmuir*, 2000, 16, 905-910.
- 26. G. Pandey and S. Dixit, *J. Phys. Chem. C.*, 2011, 115, 17633-17642.
- 27. X. Li, Y. Hou, Q. Zhao and L. Wang, J. Colloid. Interf. Sci., 2011, 358, 102-108.
- 28. S. Singhal, T. Namgyal, S. Bansal and K. Chandra, *J. Electromagnetic Analysis & Applications* 2010, 2, 376-381.
- G. Vaidyanathan, S. Sendhilnathan and R. Arulmurugan, J. Magn. Magn. Mater., 2007, 313, 293-299.
- 30. U. Resch, A. Eychmueller, M. Haase and H. Weller, *Langmuir*, 1992, 8, 2215-2218.
- 31. X. Sun, X. Ma, L. Bai, J. Liu, Z. Chang, D. G. Evans, X. Duan, J. Wang and J. F. Chiang, *Nano Res.*, 2011, 4, 226-232.
- 32. B. S. Rao, B. R. Kumar, V. R. Reddy and T. S. Rao, *Chalcogenide Lett.*, 2011, 8, 177-185.

- 33. A. Roychowdhury, S. P. Pati, S. Kumar and D. Das, *Materials Chem. and Phy.*, 2015, 115, 105-111.
- 34. P. Xiong, J. Zhu and X. Wang, *Ind. Eng. Chem. Res.*, 2013, 52, 17126-17133.
- 35. R. Sharma and S. Singhal, J Chem. Technol. Biotechnol., 2015, 90, 955-962.
- 36. R. Sharma, S. Bansal and S. Singhal, *RSC Adv.*, 2015, 5, 6006-6018.
- 37. T. Upadhyay, R. V. Upadhyay, R. V. Mehta, V. K. Aswal and P. S. Goyal, *Phys. Rev. B*, 1997, 55, 5585-5588.
- 38. S. Kumar, S. Khanchandani, M. Thirumal and Ashok K. Ganguli, *ACS Appl. Mater. Inter.*, 2014, 6, 13221-13233.
- 39. Y. Liu, L. Zhou, Y. Hu, C. Guo, H. Qian, F. Zhanga and X. W. Lou, *J. Mater. Chem.*, 2011, 21, 18359-18364.

Table 1. Average crystallite size and lattice parameter shifting of CdS nanorod-MFe₂O₄ (M = Zn, Co and Ni)

Nanocomposite	Angle (2θ)	Average crystallite size (nm)	Lattice parameter (Å)
CdS nanorods	26.804	44.166	a = 4.121 b = 6.682
ZnFe ₂ O ₄ NPs	35.406	8.1	a = 0.844
CoFe ₂ O ₄ NPs	35.661	18.7	a = 0.838
NiFe ₂ O ₄ NPs	35.865	21.5	a = 0.833

Table 2. Saturation magnetization, Coercivity and remanance of CdS nanorods-MFe $_2$ O $_4$ (M = Zn, Co and Ni) nanocomposites

Nanocomposite samples	Saturation magnetization M_s (emu/g)	Corecivity H _c (Oe)	Remanance M _r (emu/g)
CdS nanorods- ZnFe ₂ O ₄	4.0	8.5	0.005
CdS nanorods- CoFe ₂ O ₄	26.4	377	4.85
CdS nanorods NiFe ₂ O ₄	15.5	90	2.58

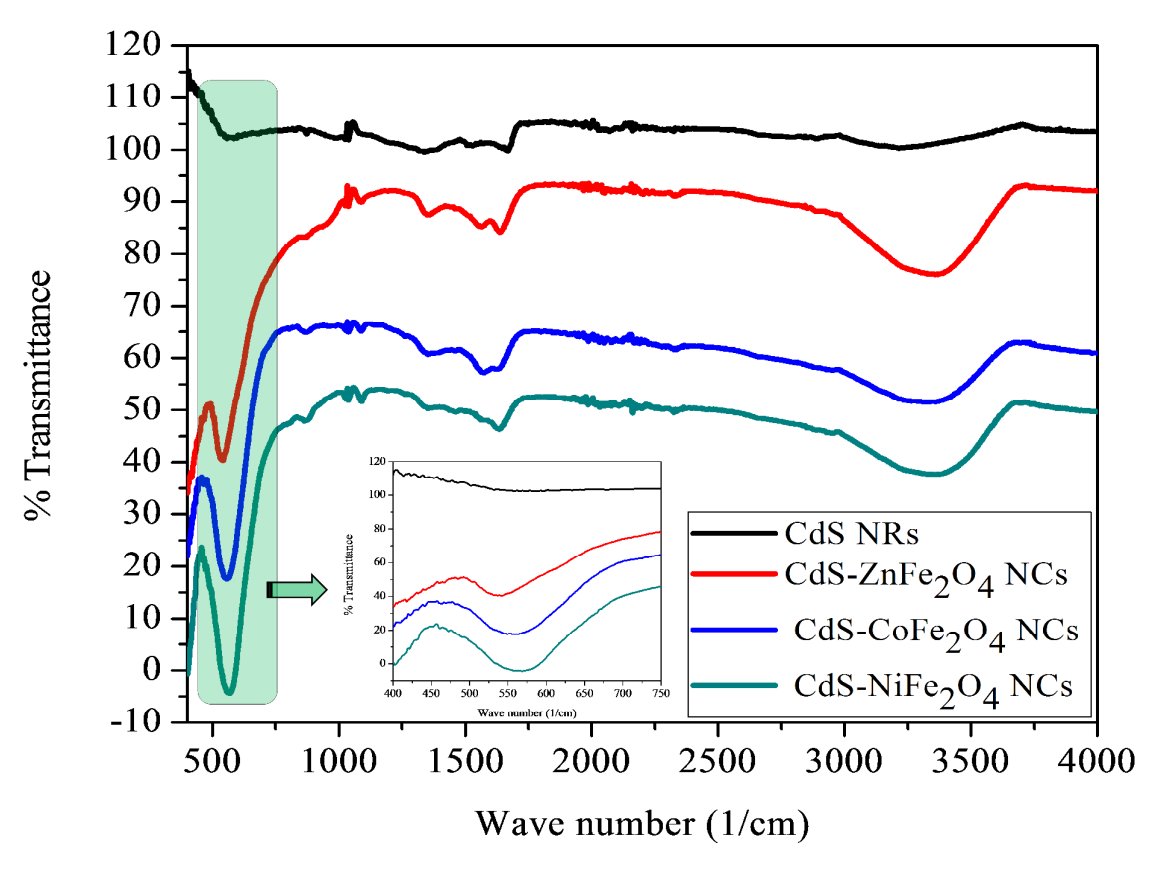


Fig 1. FT-IR spectra of CdS NRs and MFe₂O₄-CdS NCs (M = Zn, Co and Ni)

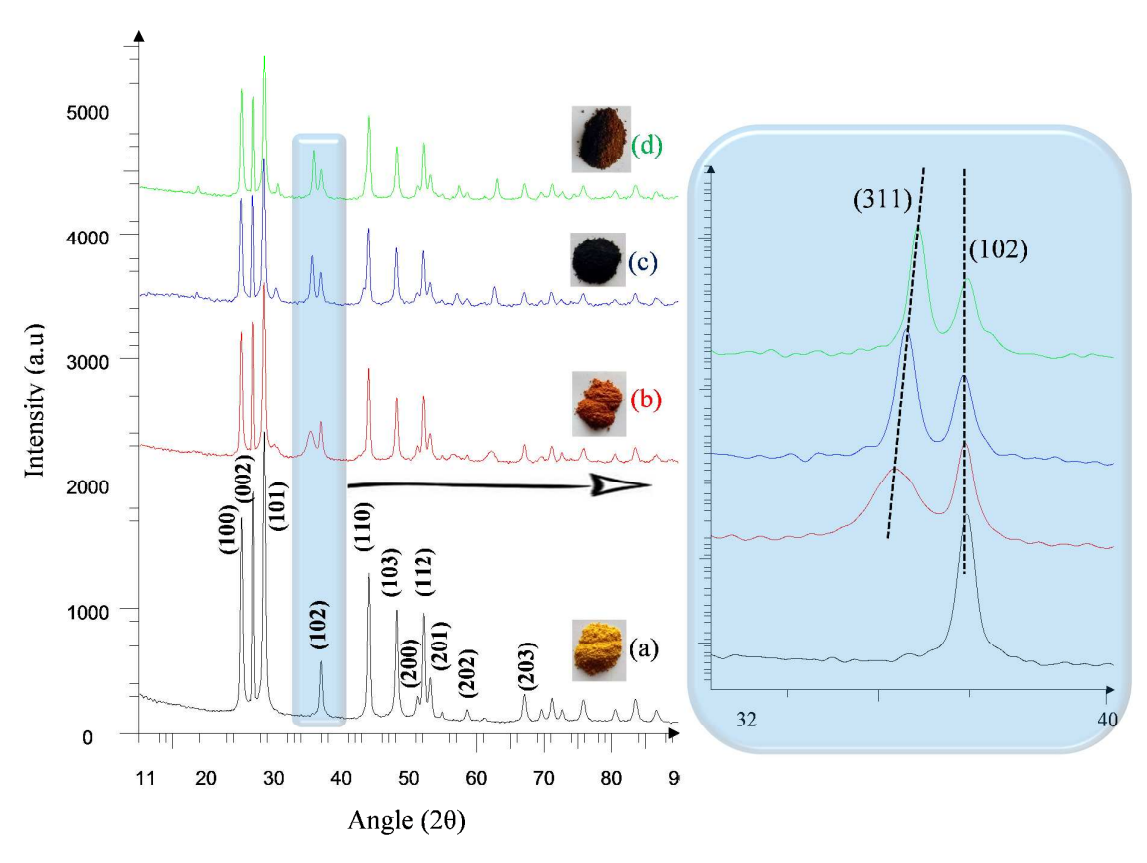


Fig 2. Typical powder XRD pattern of (a) hexagonal CdS NRs and their nanocomposites with (b) ZnFe₂O₄ (c) CoFe₂O₄ and (d) NiFe₂O₄ NPs synthesized by two step hydrothermal process (inset showing the shifting in peak corresponding to (311) plane of different ferrite-CdS NCs without disturbing the (102) plane of the hexagonal CdS NRs)

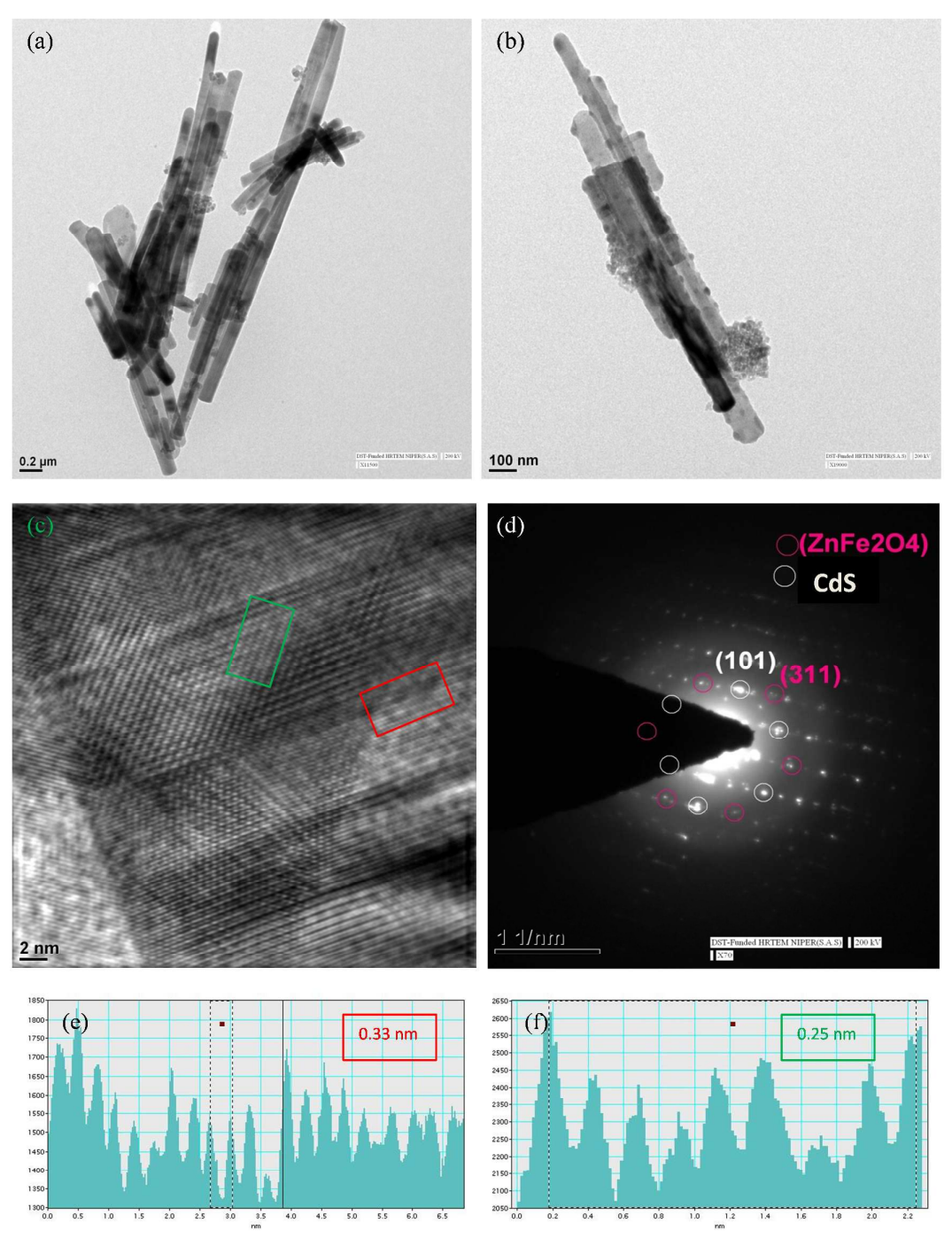


Fig 3. HRTEM image of showing the (a, b) ZnFe₂O₄ NPs loaded CdS NRs (c) high resolution image clearly interpreting the point of attachment and lattice fringes of both the domains (d) SAED pattern of the CdS NRs-ferrite NCs depicting the crystalline nature of sample (e, f) profile of frame describing the lattice fringe width

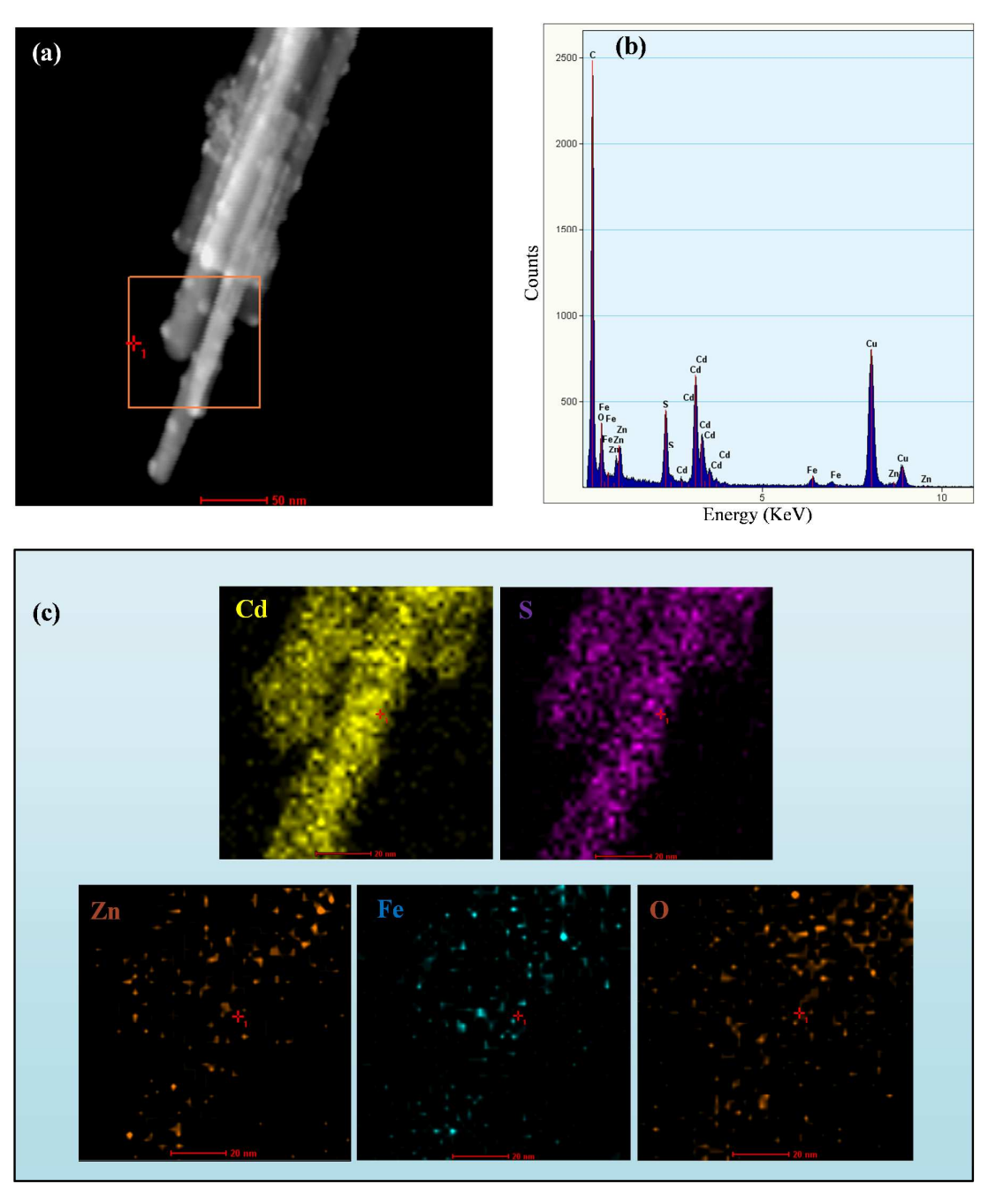


Fig 4. ZnFe₂O₄ coated CdS NRs showing the (a) STEM image for 3-D vision (b) EDX pattern showing the elemental proportion and (c) elemental mapping of Cd, S, Zn, Fe and O from the selected frame of STEM image

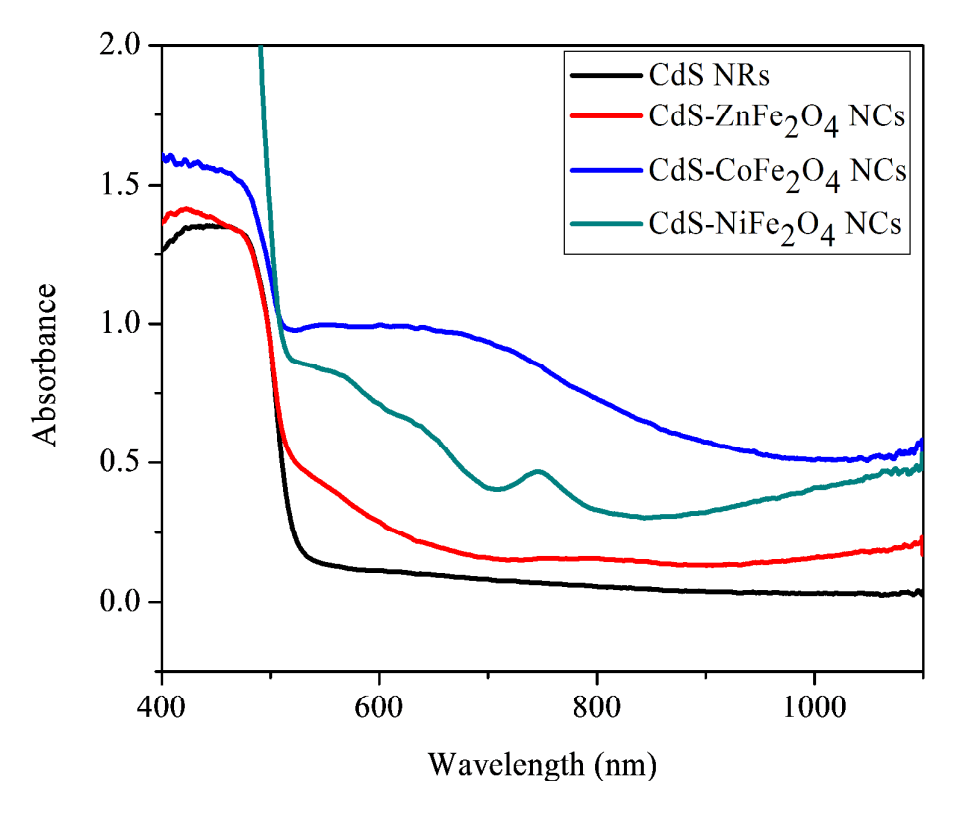


Fig 5. Diffused UV-Visible spectra of CdS NRs and nanocomposites of CdS NRs- MFe_2O_4 (M = Zn, Co and Ni) showing different band edge absorbance.

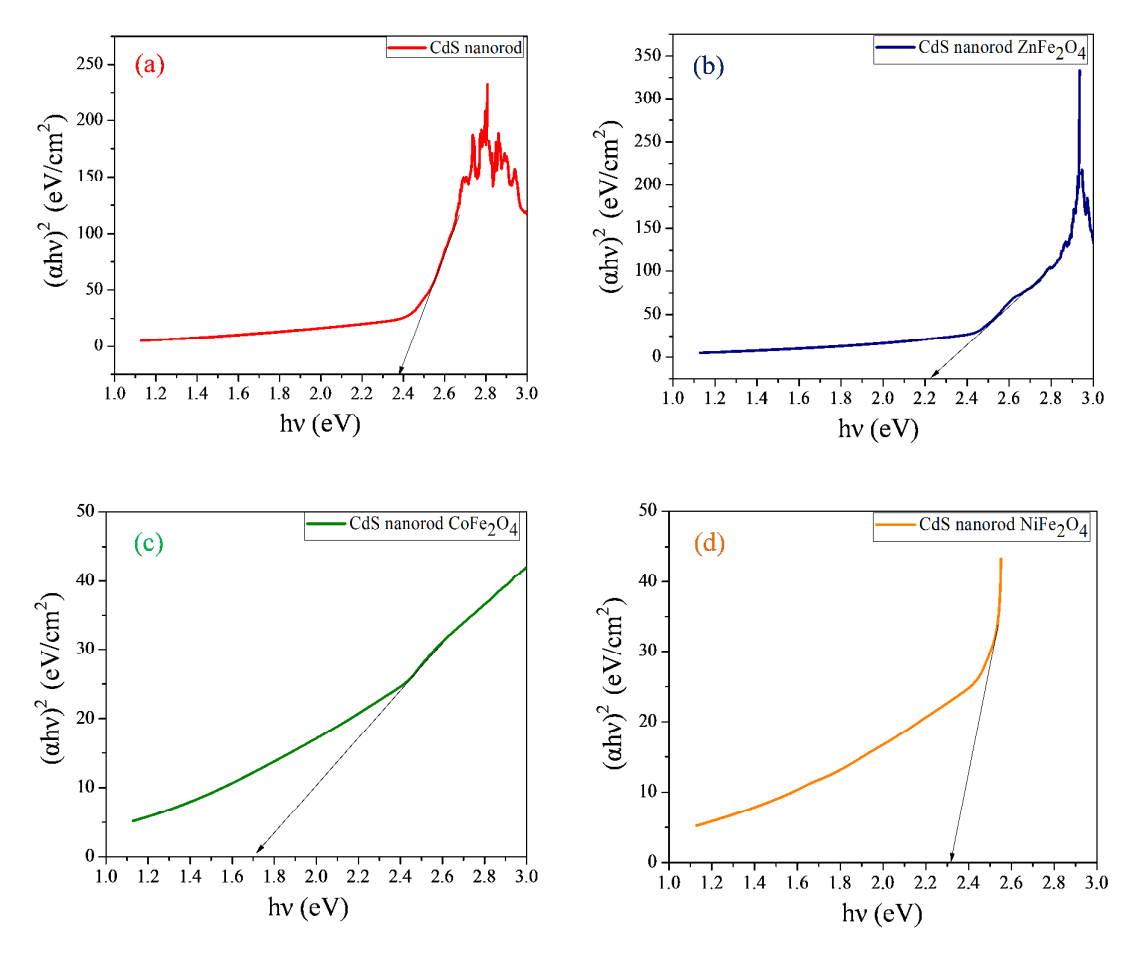


Fig 6. Plots of $(\alpha h \nu)^2$ versus hv showing the band gap of (a) CdS NRs and their nanocomposites with (b) $ZnFe_2O_4$ (c) $CoFe_2O_4$ and (d) $NiFe_2O_4$ NPs

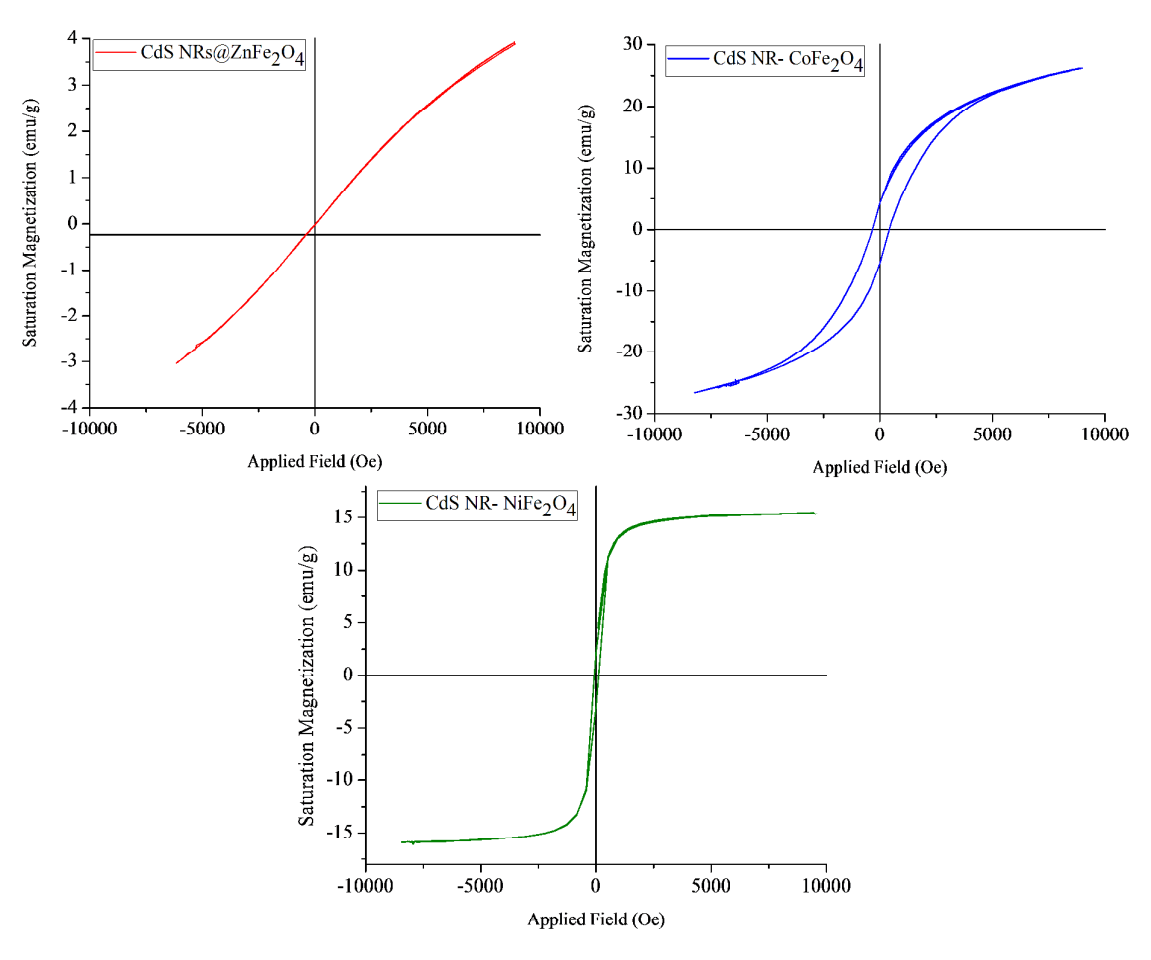


Fig 7. Magnetic hysteresis loops for CdS NR ensheathed ZnFe₂O₄, CoFe₂O₄ and NiFe₂O₄ NPs

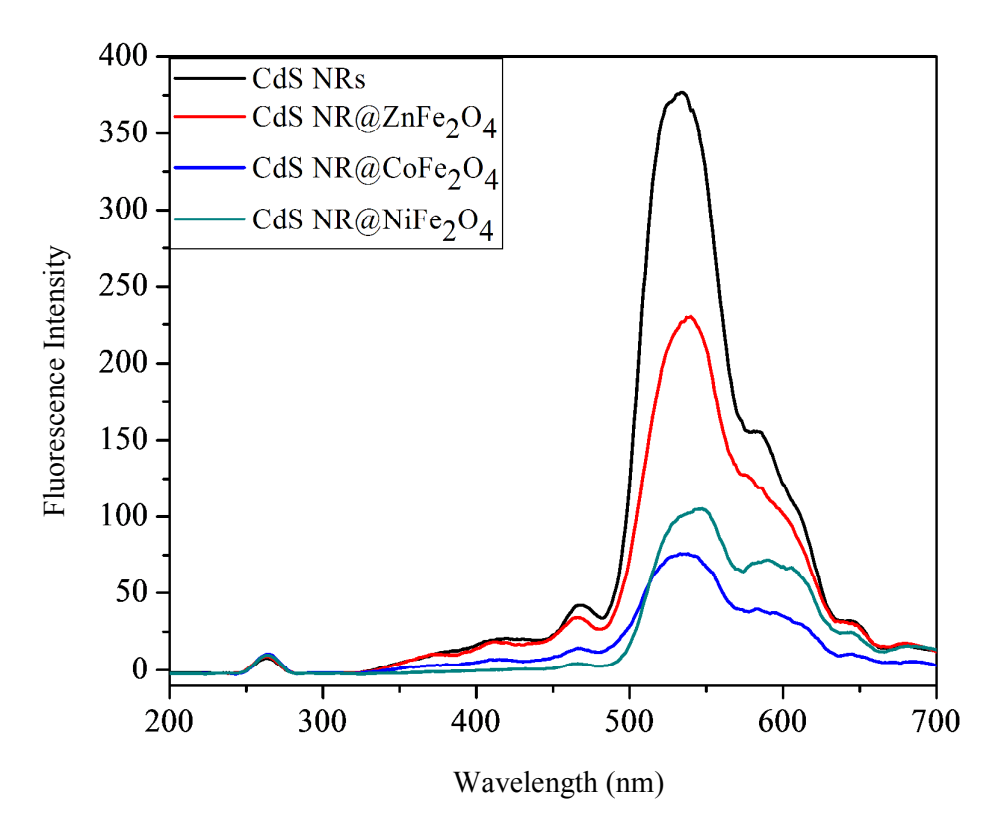


Fig.8. Photoluminescence spectra of CdS NRs and their nanocomposites with zinc, cobalt and nickel ferrite nanoparticles

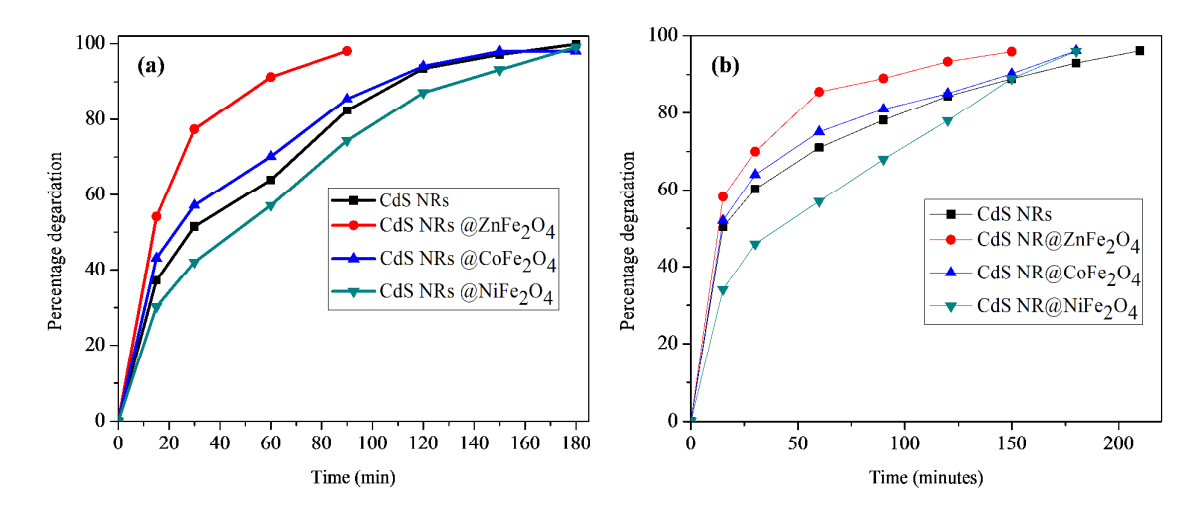


Fig 9. Percentage degradation of (a) methylene blue and (b) rhodamine B with time in the presence of CdS nanorods and their ferrite nanocomposite under visible light irradiation.